Relaxation of hot electrons in a degenerate two-dimensional electron system: Transition to one-dimensional scattering

D. Taubert,[1] C. Tomaras,[1] G. J. Schinner,[1] H. P. Tranitz,[2] W. Wegscheider,[3] S. Kehrein,[1] and S. Ludwig[1]

[1]*Center for NanoScience and Fakultät für Physik, Ludwig-Maximilians-Universität, Geschwister-Scholl-Platz 1, DE-80539 München, Germany*

[2]*Institut für Experimentelle Physik, Universität Regensburg, DE-93040 Regensburg, Germany*

[3]*Solid State Physics Laboratory, ETH Zurich, CH-8093 Zurich, Switzerland*

(Received 8 April 2011; revised manuscript received 21 April 2011; published 3 June 2011)

The energy relaxation channels of hot electrons far from thermal equilibrium in a degenerate two-dimensional electron system are investigated in transport experiments in a mesoscopic three-terminal device. We observe a transition from two dimensions at zero magnetic field to quasi-one-dimensional scattering of the hot electrons in a strong magnetic field. In the two-dimensional case, electron-electron scattering is the dominant relaxation mechanism, while the emission of optical phonons becomes more and more important as the magnetic field is increased. The observation of up to 11 optical phonons emitted per hot electron allows us to determine the onset energy of longitudinal-optical phonons in GaAs at cryogenic temperatures with a high precision $E_{\mathrm{ph}} = 36.0 \pm 0.1$ meV. Numerical calculations of electron-electron scattering and the emission of optical phonons underline our interpretation in terms of a transition to one-dimensional dynamics.

DOI: 10.1103/PhysRevB.83.235404 PACS number(s): 73.23.−b, 63.20.kd, 72.10.Di, 73.50.Gr

I. INTRODUCTION

Nonequilibrium phenomena on the nanoscale increasingly gain interest as more and more devices are based on nanoscale electronics. The ongoing miniaturization trend results in state-of-the-art transistors, used for information processing, in which only a small number of electrons is moving through a conducting channel at a given time. Semiconductor-based quantum information processing relies on the coherent dynamics in nanostructures. For both classical and, in particular, quantum circuits, the detection of information relies on electronic signals strong enough to be measurable. An inevitable consequence are interactions in nonequilibrium, giving rise to quantum noise and back-action. Our experiments aim at understanding the underlying physics of interacting nanoscale circuits where only few electrons far from thermal equilibrium carry the information.

We study in transport experiments at low temperatures the simplest case of individual nonequilibrium electrons. After their injection, these "hot" electrons move at first ballistically with well-defined, high kinetic energy before they relax in an otherwise degenerate Fermi liquid: a cold, two-dimensional electron system (2DES). We are specifically interested in the case of a high-mobility 2DES since here electrons near the Fermi edge have a momentum mean-free path l_{m} of several micrometers and therefore move ballistically through the mesoscopic device. The scattering length of the hot electrons, however, at first strongly decreases as a function of kinetic energy as the phase space for scattering processes grows. For larger kinetic energies, the electron-electron scattering length increases again because of the high velocity and short interaction times.

In a magnetic field perpendicular to the plane of the 2DES, the Lorentz force tends to guide hot electrons to move along the edges of the conducting mesa of the 2DES. In this paper, we focus on the transition between two-dimensional scattering in a low magnetic field to quasi-one-dimensional scattering in the quantum limit of edge-channel transport of the hot electrons. "Quasi-one-dimensional" refers to a situation where the lateral width of the effective transport channel still exceeds the magnetic length.

Relevant energy-loss mechanisms of hot electrons in a 2DES are the emission of plasmons, acoustic or optical phonons, or scattering with "cold" equilibrium electrons in the degenerate Fermi sea. The radiation of photons is strongly suppressed because of the momentum mismatch. The emission of plasmons by hot electrons is particularly hard to capture in pure transport experiments, so we will address plasmons only briefly from the theoretical point of view in this paper. The interaction between hot electrons and acoustic phonons constitutes a minor contribution to the relaxation of hot electrons in our nonequilibrium experiments. It therefore will not be a focus here, but detailed investigations in zero magnetic field have already been conducted on comparable samples by using a phonon spectroscopy technique.[1] It is worth mentioning, however, that acoustic phonons play a major role in interactions between *electrically separated* nanostructures in nonequilibrium without[2–6] and with[7] a perpendicular magnetic field applied.

The emission of optical phonons has been studied in zero magnetic field in various types of experiments since the 1960s. It usually shows up as a very weak oscillatory signal as a function of the kinetic energy of hot electrons, with an oscillation frequency equal to the phonon energy. It has been observed in several materials, including GaAs, in photoconductivity,[8–11] in Raman scattering experiments,[12] as well as in pure transport experiments in which electrons tunnel vertically between layers of a heterostructure.[13–17] Later, the emission of optical phonons has also been observed in lateral devices defined in GaAs-based heterostructures.[18,19]

The scattering of hot electrons in zero magnetic field with a cold 2DES has been experimentally investigated in lateral three-terminal devices, where the three regions have been separated by electrostatic barriers.[19–23] It has been demonstrated that the electron-electron interaction in such mesoscopic three-terminal devices gives rise to effects such

as a "negative resistance"[19] and can be used for avalanche amplification of a current of hot injected electrons.[22,23]

Building on Refs. 22 and 23, we find that the transition from two- to one-dimensional scattering, as a perpendicular magnetic field is increased, goes along with a change in the importance of electron-electron scattering versus the emission of optical phonons. These two processes dominate the scattering dynamics of hot electrons in a degenerate two- or one-dimensional electron system in the whole range of available magnetic fields. At low fields, hot electrons relax mainly via electron-electron scattering, while the emission of optical phonons becomes more and more important at high fields. Still, amplification of the injected electron current based on electron-electron scattering occurs even in a large perpendicular magnetic field. Our measurements indicate that the scattering time between hot electrons and optical phonons strongly decreases as a function of the perpendicular magnetic field, while the electron-electron scattering time increases. Our experimental results are backed up by numerical calculations of the electron-electron scattering time and the emission rate of optical phonons as a function of the perpendicular magnetic field. Finally, changing the magnetic-field direction reveals a contribution of hopping transport via high-energy localized bulk states of the 2DES where a strong perpendicular magnetic field hinders the screening of disorder.

II. SAMPLE AND SETUP

Our sample is based on a GaAs/AlGaAs heterostructure with a 2DES 90 nm below the surface. The charge carrier density is $n_s = 2.7 \times 10^{11}$ cm^{-2}, which corresponds to a Fermi energy of $E_F = 9.7$ meV (determined at a temperature of $T = 260$ mK). Its electron mobility (measured at the temperature $T = 1$ K) is $\mu = 1.4 \times 10^6$ cm^2/(Vs). The resulting equilibrium momentum mean-free path is $l_m \simeq 12\,\mu$m, an order of magnitude longer than the relevant distances in our sample. A Hall-bar–like mesa, visible as an elevated area in the scanning electron micrograph in Fig. 1(a), was created by electron-beam lithography and wet etching. The device has several ohmic contacts, three of which are used in the experiments as the emitter "E," the collector "C," and an additional "side" contact. Seven metal electrodes [not all of them are visible in Fig. 1(a)] have been fabricated by electron-beam lithography and evaporation, and are used to create electrostatic barriers by applying gate voltages. The two barriers used here are named emitter barrier BE and collector barrier BC. The latter has been designed as a broad (300 nm gate width) classical barrier, whereas the former is actually a quantum point contact. Note that the exact nature of the emitter is not important in the experiments shown here (similar measurements with a broad barrier as emitter yield comparable results). The sample was measured in a ^{3}He cryostat at an electron temperature of $T \sim 260$ mK.

Unless stated otherwise, a negative dc voltage is applied to the emitter contact while the dc currents I_{side} and I_C flowing into the grounded collector and side contacts are measured with low noise current amplifiers. The electric potentials on all other ohmic contacts of the nanostructure are left floating. Great care was taken to tune the voltage offsets at the inputs of both current amplifiers to zero and, hence, avoid a superimposed current between side contact and collector.

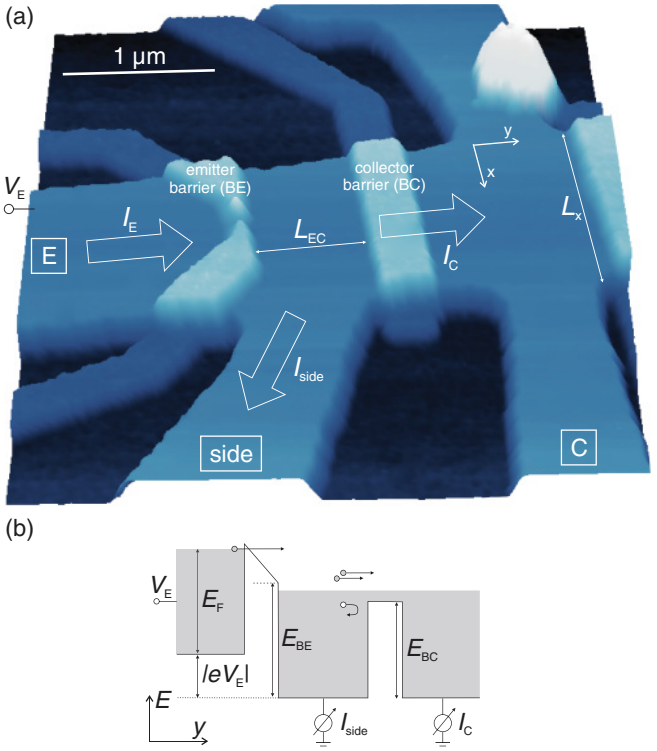

FIG. 1. (Color online) (a) Atomic force micrograph of the sample. The elevated areas still contain a 2DES below the surface, which is removed by wet-etching elsewhere. In addition, metal electrons are visible on top of the Hall bar marked as emitter (BE) and collector (BC). (b) Model that explains the avalanche amplification effect, which is based on scattering of hot electrons with the degenerate Fermi sea of the 2DES at low temperatures.

The emitter current I_E is derived via Kirchhoff's current law $I_E = I_{side} + I_C$, where we define the three currents to be positive if electrons flow into the sample from the emitter and leave the sample at the side contact and the collector [compare arrows in Fig. 1(a)]. This scenario would be expected in the limit of diffusive transport for which the sample can be described as a network of ohmic resistors.

III. AVALANCHE AMPLIFICATION

Electron-electron scattering can cause major deviations from this ohmic case, as we have already discussed in detail in Refs. 22 and 23. The following paragraph gives a brief overview of their main results. We keep the emitter barrier BE nearly pinched off and hence almost the entire voltage V_E applied to the emitter drops across BE. All electrons injected via BE into the central region of the sample then have an excess kinetic energy $E_{kin} - E_F$ close to $|eV_E|$ because of the barrier's transmission probability that depends exponentially on energy. These *hot* electrons then excite via electron-electron scattering *cold* electrons, which leave behind unoccupied states in the otherwise degenerate Fermi sea. If we name these unoccupied states in the conduction band "holes" (not to be confused with valence-band holes), the scattering process far from thermal equilibrium, schematically depicted in Fig. 1(b), can be interpreted as excitation of electron-hole pairs. If BC is configured such that excited electrons can pass, but most

holes are reflected, the positively charged holes will reside between BE and BC until they will eventually be neutralized by electrons drawn in from the side contact. (For charge separation to work effectively, BC has to be slightly below the Fermi energy. See Ref. 23 for a detailed explanation.) In its extreme, this can cause $I_E < 0$ and consequently $I_C > I_E$, where more electrons leave the device at the collector compared to the number of injected electrons. This is the case of avalanche amplification of the injected current.

Figures 2(a) and 2(b) depict I_{side} and I_C measured as the gate voltage V_{BE} (x axis), defining the emitter barrier BE, and the bias voltage V_E (y axis) have been varied. Data are only taken in the regime of BE nearly pinched off, namely, within the roughly diagonal stripe of the graph with variable color. The upper left regions of the two plots (gray) are characterized by $I_E = I_{side} = I_C = 0$ and have therefore not been mapped out in detail. To prevent excessive heating of the sample, the overall dissipated power has been limited to $I_E V_E \leqslant 700$ nW, which results in no data for the lower right regions (also gray) of Figs. 2(a) and 2(b). The gate voltage V_{BE} controls the emitter current I_E while the injected electrons have an energy close to $E_{kin} = E_F + |eV_E|$. Within the measured area of Fig. 2(a), a narrow stripe of $I_{side} < 0$ is visible in which amplification of the injected current occurs.[22]

Figure 2(c) shows the amplification effect in a more instructive way. The raw data from Fig. 2(a) is plotted as a function of the injected current I_E and the bias voltage V_E. The area of negative side current is enclosed by the dashed contour line marking $I_{side} = 0$. Other contour lines of constant current are white at $I_{side} < 0$ and black at $I_{side} > 0$. I_{side} strongly depends on the energy of the injected electrons. This behavior is caused by the energy dependence of the electron-electron scattering length $l_{e\text{-}e}(eV_E)$. Near its absolute minimum at $|eV_E| \simeq 150$ meV, $l_{e\text{-}e}$ is actually smaller than the distance L_{EC} between BE and BC.[22] In this regime, multiple scattering processes lead to the excitation of a large number of electron-hole pairs between BE and BC. If only excited electrons with $E_{kin} > E_F$ can escape via BC (tuned to a barrier height near the Fermi edge), a positive charge can build up between BE and BC, which results in $I_{side} < 0$ as the side contact is grounded.

At a slightly larger energy of the injected electrons, our data suggest $l_{e\text{-}e} \gtrsim L_{EC}$,[22] meaning that scattering tends to happen just beyond the collector barrier. In this regime, electrons can be backscattered from behind BC, and then leave the sample at the grounded side contact. This manifests itself in a positive side current and a small, in some cases even negative, collector current. The latter can be seen in Fig. 2(b) or better 2(d), which shows I_C as a function of I_E and V_E in the same fashion as for I_{side} in Fig. 2(c). In Figs. 2(c) and 2(d), the positive I_{side} and rather small I_C are clearly visible as ridgelike structures at $|eV_E| \sim 300$ meV (see contour lines).

For $|V_E| > 350$ mV, we find $I_{side} \simeq 0$ [Fig. 2(a)]. This can be interpreted in terms of $l_{e\text{-}e}$ exceeding the sample dimensions so that the injected electrons pass the device without electron-electron scattering. Most injected electrons then move ballistically into the collector contact.[22] Figure 2(e) shows the current transfer ratio defined as $\alpha = I_C/I_E$ for the same set of data as in the other subfigures. The maximal value observed in the data presented here is $\alpha \simeq 4.5$, although we have already reached higher amplification factors of $\alpha \simeq 8$ in a different sample. $I_{side} \simeq 0$ in the high-energy region in Fig. 2(a) corresponds to $\alpha \simeq 1$ and $I_C \simeq I_E$ in Figs. 2(e) and 2(d), respectively.

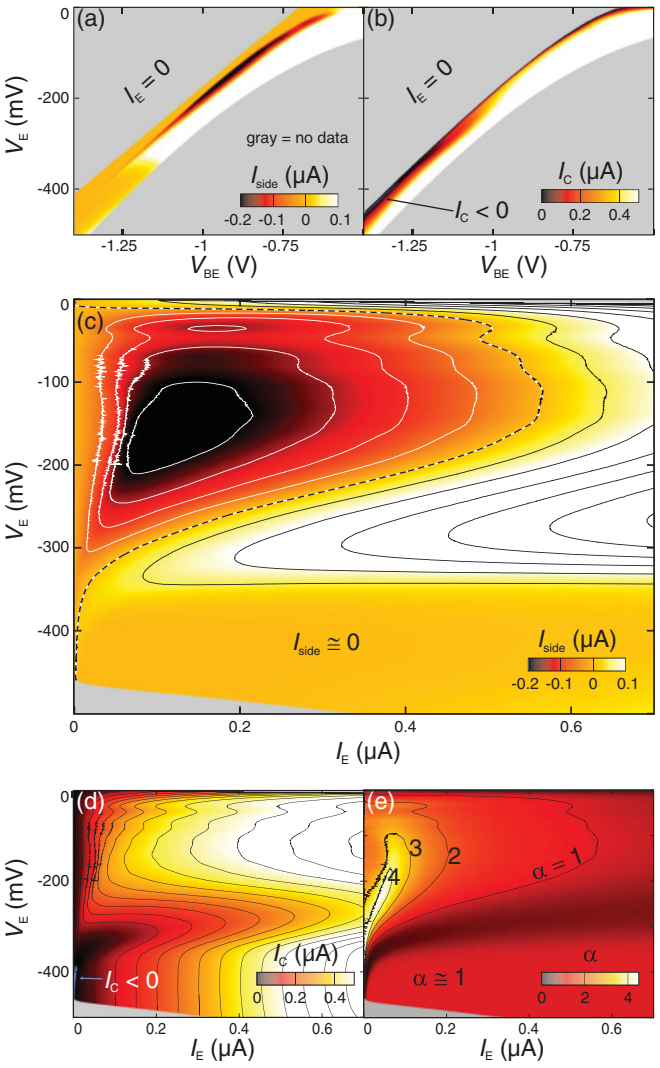

FIG. 2. (Color online) Measurements at constant $V_{BC} = +45$ mV ($E_{BC} = E_F - 1.5$ meV; see Ref. 23 for details on determining the barrier height in units of energy). (a), (b) I_{side} and I_C as a function of V_{BE} and V_E. (c) I_{side} as in (a), but plotted as a function of the injected current I_E instead of V_{BE}. An extended region at the bottom ($|V_E| > 350$ mV) has $I_{side} \simeq 0$ (see Ref. 23 for details). Contour lines are spaced by 50 nA; white for $I_{side} < 0$, black for $I_{side} > 0$, and dashed line for $I_{side} = 0$. (d) Collector current, same type of plot as in (c). A very small area of $I_C < 0$ is marked in the bottom left corner. (e) Current transfer ratio $\alpha = I_C/I_E$, same axes. Contour lines at $\alpha = 1,2,3,4$; the extended range of constant current at the bottom corresponds to $\alpha \simeq 1$.

Note that the highest excess kinetic energies studied here, up to $E_{kin} \simeq 500$ meV, are large compared to the Fermi energy of $E_F \simeq 9.7$ meV and also exceed the energy of optical phonons ($E_{ph} \simeq 36$ meV in GaAs) by far. In the data presented in Fig. 2(c), the emission of optical phonons is faintly visible as "wiggles" in the contour lines with extrema at $V_E = 36$ and 72 mV. Optical phonons will be discussed in detail in Sec. V

in the context of a magnetic field applied perpendicularly to the plane of the 2DES.

It should be mentioned that the energy range used for the hot electrons in our experiments also exceeds the intersubband energy of the 2DES, which is in the order of 30 meV. Nevertheless, we do not observe any signatures of intersubband scattering, which, therefore, seems to be inefficient compared to intrasubband scattering. Most probably, the majority of hot electrons still occupy the lowest subband that they used to populate in the emitter contact before being injected across BE. Moreover, the maximum energy of $|eV_E| = 500$ meV is even larger than the vertical confinement energy of the 2DES, which could cause scattering of hot electrons into three-dimensional bulk states. We have not observed any signatures of transport through the bulk of the heterostructure in our experiments, though.

IV. FROM TWO DIMENSIONS TO ONE-DIMENSIONAL ELECTRON-ELECTRON SCATTERING IN A PERPENDICULAR MAGNETIC FIELD

A. Magnetic-field dependence of electron-electron scattering

In a magnetic field B perpendicular to the plane of the 2DES, the Lorentz force $\vec{F}_L = e\vec{v} \times \vec{B}$ acts on electrons perpendicularly to their momentary velocity $\vec{v}$ and forces them to move along the edges of the conducting mesa. In a simple classical picture, ballistic electrons are again and again reflected at the edge and move along well-defined skipping orbits with the cyclotron radius $R_c = |\vec{v}|/\omega_c$ and the cyclotron frequency $\omega_c = |eB|/m_{\rm eff}$, where $m_{\rm eff}$ is the effective mass of the electrons. This classical limit has indeed often been observed in magnetic focusing experiments close to equilibrium and in moderate magnetic fields (an example including nonequilibrium scattering is Ref. 24). In a quantum-mechanical description, the angular-momentum quantization only allows cyclotron radii with $R_c(n) = \sqrt{2(n+0.5)}\,l_c$, which, for $n = 0$, is equal to the so-called magnetic length $l_c = \sqrt{\hbar/|eB|}$, and where $n = 0,1,2,\ldots$ is the Landau level index. For the case of $E_{\rm kin} \sim E_F$ and strong quantization (small n), the Landauer-Büttiker description of the quantum Hall effect has often been used. This model assumes a nondissipative one-dimensional motion of current-carrying electrons within edge channels.[25] While in the past electrons close to thermal equilibrium have been studied in a perpendicular magnetic field, here we are interested in hot electrons far from thermal equilibrium with $E_{\rm kin} \gg E_F$. In the following, the Landau level n therefore pertains to the energy of the hot electrons rather than the number of filled Landau levels in a degenerate 2DES. In this nonequilibrium situation, we aim at observing the transition from a two-dimensional electron system (large R_c and large n) to the case of one-dimensional motion (small R_c and small n) in a strong perpendicular magnetic field. Since $R_c \propto |\vec{v}/B|$, we expect to observe one-dimensional behavior to occur at sizable magnetic fields and not too large kinetic energies of the hot electrons.

To achieve this, we have extended the previous results[22,23] summarized above by applying a perpendicular magnetic field. Figure 3(a) shows a measurement analogous to Fig. 2(c), but in a magnetic field of $B = 4.7$ T, which corresponds to a filling factor of $\nu \simeq 1.9$ [$n = \text{int}(\nu/2) = 1$] for equilibrium electrons at the Fermi energy. The raw data are shown as inset analogously to Fig. 2(a). We define the sign of B to be positive for B directed upward, i. e., such that electrons injected via BE into the sample are guided to the left, away from the side contact [Fig. 1(a)]. The influence of the field direction will be discussed in detail in Sec. VI. Compared to the case of no magnetic field applied, at $B = 4.7$ T, the emitter current is slightly reduced (by about 20%). This is related to the conductance quantization and corresponding increase of

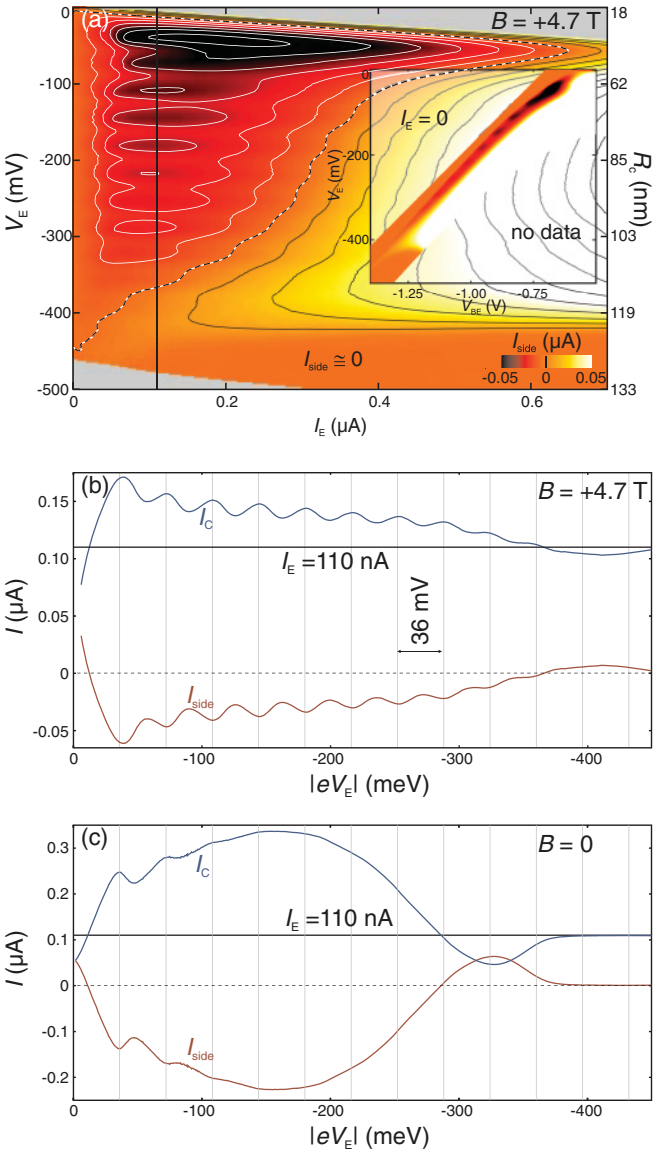

FIG. 3. (Color online) (a) Side current as a function of injected current I_E and bias voltage V_E in a perpendicular magnetic field of $B = 4.7$ T; contour lines are spaced by 10 nA and colored as in Fig. 2(c). The inset shows the raw data as a function of V_E and V_{BC} [as for $B = 0$ in Fig. 2(a)]. (b) I_{side} and I_C as a function of the excess energy $|eV_E|$ of the injected electrons for a constant $I_E = 110$ nA [horizontal solid line, vertical line in Fig. 3(a)]. (c) Energy dependence of the currents as in (b), but for $B = 0$ [vertical trace of Fig. 2(c) for $I_E = 110$ nA]. Vertical lines in (b) and (c) are spaced by $E_{ph} = 36$ meV.

the resistance of a 2DES in a strong perpendicular magnetic field. However, the absolute value of the minimum of $I_{\rm side}$ and the maximum of α (the current transfer ratio) are much more reduced, roughly by factors of 4 and 2, respectively [compare Figs. 2(c) and 3(a)].

A notable difference compared to zero magnetic field is that, for $B = 4.7$ T, $I_{\rm side}$ is strongly modulated with a period close to $\delta E = 36$ meV. The oscillations of $I_{\rm side}$ are also mapped onto $I_{\rm C}$ as can best be seen in Fig. 3(b), which plots both currents as a function of $|eV_{\rm E}|$ for a fixed $I_{\rm E} = 110$ nA [marked by a vertical line in Fig. 3(a) and a horizontal line in Fig. 3(b)]. These oscillations are caused by the emission of optical phonons with an energy $E_{\rm ph} \simeq 36$ meV and will be discussed in detail in Sec. V. The analogous measurement for $B = 0$ shown in Fig. 3(c) allows a quantitative comparison near maximum amplification. At zero magnetic field, amplification clearly is much stronger (deeper minimum of $I_{\rm side}$), while phonon-induced oscillations are only seen at relatively small energies of $|eV_{\rm E}| \lesssim 100$ meV. These observations imply that, in our sample, the electron-electron scattering rate between BE and BC decreases in a perpendicular magnetic field while at the same time the emission of optical phonons becomes more significant.

Furthermore, the shape and current profile of the region of $I_{\rm side} < 0$ [framed by dashed contour lines in Figs. 2(c) and 3(a)], corresponding to $\alpha > 1$, changes drastically if a perpendicular magnetic field is applied. For relatively small injected currents $I_{\rm E}$ the region of $I_{\rm side} < 0$ extends toward larger $|eV_{\rm E}|$ in a perpendicular magnetic field. At the same time, the absolute minimum of $I_{\rm side}(V_{\rm E})$, which is relatively broad at $B = 0$, shifts toward smaller energies $|eV_{\rm E}| < 100$ meV and narrows in a magnetic field. This first (and deepest) minimum of $I_{\rm side}$ due to optical phonons at $B = 4.7$ T still extends to relatively large currents up to $I_{\rm E} > 0.6\ \mu$A. With increasing $I_{\rm E}$ the main minimum shifts toward larger $|eV_{\rm E}|$ while the phonon-induced oscillations are constant in $|eV_{\rm E}|$. We conclude that, in a large perpendicular magnetic field, the dependence of the amplification effect on the energy $|eV_{\rm E}|$ is strongly altered by the emission of optical phonons while its dependence on the dissipated power $P = I_{\rm E}V_{\rm E}$ is still dominated by electron-electron scattering.

Could the observed change in the amplification effect then be related to a transition of scattering of hot electrons in two dimensions to one-dimensional scattering at finite B? A first answer to this question can be given by a comparison of the screening length $k_{\rm F}^{-1} \simeq 8$ nm of the 2DES at $B = 0$ with the width of the current-carrying channel at $B = 4.7$ T, approximately given by the cyclotron radius in the quantum Hall regime. At $B = 4.7$ T, we find $R_{\rm c}(n = 1) = l_{\rm c} \simeq 12$ nm, which is in the same order of magnitude as $k_{\rm F}^{-1}$. The main minimum of $I_{\rm side}$ in Fig. 3(a) at relatively large currents, where the phonon-induced oscillations are weak, occurs at energies in the order of $|eV_{\rm E}| \sim 50$ meV. This corresponds to $R_{\rm c} \geqslant 45$ nm (and $n \simeq 7$), which is considerably larger than the two-dimensional screening length $k_{\rm F}^{-1} \simeq 8$ nm. Hence, we do not expect our data to resolve the complete transition from two-dimensional to fully one-dimensional scattering of hot electrons. The comparison of the length scales suggests that our data can be interpreted as a signature of quasi-one-dimensional scattering.

B. Hot electron statistics

We start a more detailed discussion by highlighting some numbers relevant for the scattering dynamics of the hot electrons. In the next two sections, we will then present theoretical considerations pertaining to scattering of hot electrons with a degenerate 2DES in a perpendicular magnetic field. The area occupied by 2DES between BE and BC measures slightly more than a square micrometer and, therefore, contains about 3000 electrons. The potential in this area is increased in a regime of avalanche amplification by up to $\delta V \sim 1$ mV (see Ref. 22 for details on the setup used to obtain this number), which corresponds to a reduction of the resident electrons by roughly 10%. In the following, we restrict the discussion to effects at considerably larger energy scales.

For simplicity, we now assume that the injected electrons move ballistically from BE to BC across the distance of $L_{\rm EC} \simeq 700$ nm. Then, the average number of hot electrons traveling simultaneously between BE and BC is $\langle N\rangle = |\frac{I_{\rm E}L_{\rm EC}}{e}|\sqrt{\frac{m_{\rm eff}}{2(E_{\rm F}+|eV_{\rm E}|)}}$. We find a maximum of $\langle N\rangle \simeq 10$ for our measurements at $I_{\rm E} = 0.6\ \mu$A and $V_{\rm E} = -10$ meV. However, amplification ($I_{\rm side} < 0$) occurs at $\langle N\rangle \lesssim 1$ and most of the following discussions apply to this case for which we can neglect direct Coulomb interaction between hot electrons.

C. The role of plasmons

Scattering of hot electrons with a three-dimensional degenerate electron system is discussed in standard textbooks on Landau-Fermi–liquid theory.[26–28] In three dimensions, an energy-dependent quasiparticle relaxation that can be divided into two regimes is usually considered. On the one hand, the relaxation of excited electrons at rather low energies with momenta $k \ll 2k_{\rm F}$ is dominated by particle-hole excitations. On the other hand, at rather high energies (in the order of several electron volts in typical metals) beyond the plasma frequency, the emission of plasmons becomes important. In two dimensions, this clear separation into two regimes breaks down at relatively high electron densities for which the Fermi energy $E_{\rm F}$ by far exceeds the mean mutual Coulomb energy $\langle E_{\rm C}\rangle$ between conduction-band electrons (and the Thomas-Fermi wavelength exceeds the interparticle distance): $r_{\rm s} \equiv \frac{\langle E_{\rm C}\rangle}{E_{\rm F}} \propto 1/\sqrt{n_{\rm s}}$ fulfills $r_{\rm s} \ll 1$.[29,30] Our sample resides with $r_{\rm s} \simeq 0.6$ in an intermediate regime and we expect that the relaxation of hot electrons with sizable excess energies via the emission of plasmons should play a role at zero magnetic field. Nevertheless, our transport measurements have proven to be relatively insensitive to the emission of plasmons, and we have not been able to identify traces of plasmon excitations in our present data.

If, in addition, a perpendicular magnetic field B is applied, the two-dimensional bulk electrons become rigid against perturbations at energies low compared to the Landau-level separation $\hbar\omega_{\rm c}$. For hydrodynamic plasmons, i. e., in the limit of very small momenta $q \to 0$, the only difference between the two cases of $B > 0$ and $B = 0$ is this finite gap $\hbar\omega_{\rm c}$.[31–36]

However, at sufficiently high magnetic field, the transport properties of a disordered 2DES are determined by the one-dimensional edge channels, hence, the bulk magnetoplasmons would not be visible in a transport measurement. In a one-dimensional system, interactions are strong and the electron system can be described as a Luttinger liquid rather than a Landau-Fermi liquid. In the low-energy regime, the relaxation is dominated by dephasing.[37,38] For technical reasons, investigations of the electron-plasmon interaction in the Luttinger liquid are limited to intermediate energies corresponding to momenta $k \lesssim 2k_F$.[39,40] One would expect that the scattering of a single hot electron with the degenerate electron system displays a transition from Landau-Fermi to Luttinger liquid behavior as the external magnetic field is increased. This feature is absent in the present experiment, which can be understood by considering the width of the one-dimensional channel as described in the following.

D. Magnetic-field-dependent calculations

Here, we calculate the electron-electron scattering length of hot electrons moving in a quasi-one-dimensional channel of an otherwise degenerate 2DES. The width of the quasi-one-dimensional edge channel, produced by a perpendicular magnetic field, is approximately given by the cyclotron radius $R_c = \sqrt{2(n+0.5)}\,l_c$. We specifically consider the realistic scenario of weak two-dimensional scattering in which the width of the channel exceeds the screening length of the 2DES by far, $R_c \gg k_F^{-1}$.

Edge channels form in a perpendicular magnetic field because the physical edges of the Hall bar represent boundaries that bend the Landau levels upward in energy. Formally, the degeneracy of the electrons in each Landau level is lifted near the edges according to $E_n = E_n(p_y)$, where p_y denotes the momentum component of a hot electron parallel to the edge of the 2DES. A good approximation for etched edges is a hard-wall confinement of the 2DES, which allows an exact calculation of the dispersion[41]

$$E_n(p_y) = \left(n + \frac{1}{2}\right)\hbar\omega_c + \frac{p_y^2 - p_{\min}^2}{2l_c^2}\,\Theta\left(\frac{p_y^2 - p_{\min}^2}{2l_c^2}\right). \quad (1)$$

The resulting single-electron wave functions resemble those of the free 2DES, $\Psi_n(p_y) \sim H_n(x - l_c^2 p_y)e^{ip_y y}$, with H_n being the nth Hermite function. The electrons within the quasi-one-dimensional channel interact via the two-dimensional Coulomb potential

$$\widehat{V}_{2D} = \sum_{\vec{q},\vec{k},\vec{p}} v(|q|) \sum_{nmn'm'} |J_{mn}(q_y,q_x,0)|^2 \times c^\dagger_{\vec{k}+\vec{q}|m,\sigma} c^\dagger_{\vec{p}-\vec{q}|n,\bar{\sigma}} c_{\vec{p}|m',\bar{\sigma}} c_{\vec{k}|n',\sigma}\,, \quad (2)$$

where $c^\dagger_{\vec{k}|m,\sigma}$ creates an electron with momentum $\vec{k}$ in the nth Landau level, $v(|q|)$ is the ordinary two-dimensional Coulomb matrix element with the exchange momentum $\vec{q}$, and $J_{mn}(q_x,q_y,0)$ describes the interaction between electrons in the Landau levels n and m. Further details have been discussed in Ref. 36. In the limit of hydrodynamic transitions, i.e., $q \to 0$, Eq. (2) reduces to the ordinary plane-wave Coulomb interaction. Giuliani *et al.* calculated the electron-electron scattering rate at $B = 0$.[29] It is straightforward to write down the analog in the presence of a perpendicular magnetic field

$$\frac{1}{\tau_m(p_y)} = \sum_{\vec{q},m,n} \left[\frac{v(|\vec{q}|)|J_{mn}(q_y,q_x,0)|^2}{\pi\epsilon_{RPA}[q, E_m(p_y) - E_n(p_y+q_y)]}\right]'' \times [1 - f_n(p_y+q_y)] \quad (3)$$

by summing over those exchange momenta $\vec{q}$ that are related to electron-electron interaction within the quasi-one-dimensional channel ($|q| \sim 2\pi n/l_c$). Here, the dielectric susceptibility $\chi_0 = (1 - \epsilon_{RPA})/v(|\vec{q}|)$ is given by

$$\chi_0(q,\omega) = \sum_{mn,k} |J_{mn}(q_y,q_x,0)|^2 \times \frac{f_m(k) - f_n(k+q_y)}{\omega - i0^+ + E_m(k) - E_n(k+q_y)}\,, \quad (4)$$

and momentum sums are cut off at $p_{max} = L_x/2l_c^2$, where L_x is the width of the Hall bar (see Fig. 1); f_n is the Fermi distribution in the nth Landau level. For our numerical evaluation, we use the quadratic dispersion in Eq. (1), which is the exact solution for a hard-wall confinement. Since a clear physical separation of the edge channels at high energies seems unlikely, we assume that each *in situ* injected electron with energy E_{kin} occupies any one of the Landau levels fulfilling $E_{kin} < E(n,p_y)$ with equal probability and average the inverse quasiparticle lifetime over these channels.

In Fig. 4, we show the electron-electron scattering length $l_{e\text{-}e} = |\vec{v}|\tau_{ee}$ calculated with Eq. (4) for the $n = 1,2,3$ Landau

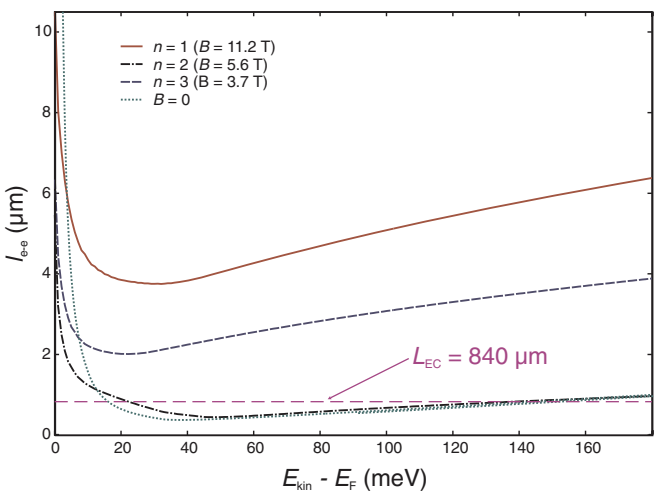

FIG. 4. (Color online) Calculated scattering length for scattering between one hot electron with kinetic energy E_{kin} and cold electrons of the degenerate 2DES as a function of excess kinetic energy for different filling fractions with fully occupied Landau levels $n = 1,2,3$ and $n \to \infty$ (corresponding to $B = 0$). To compare the values of n with experimental data, corresponding values of B are given as well, calculated for the charge carrier density of our sample.

levels fully occupied by the degenerate 2DES (integer filling factors $\nu = 2,4,6$) as well as the $B = 0$ result (corresponding to $n \to \infty$) obtained in a previous calculation.[22] The overall shape of all curves is similar, exhibiting a rapid decrease of $l_{e\text{-}e}$ for $k \ll 2k_F$ followed by a gradual increase of $l_{e\text{-}e} \propto E_{kin}$ in the limit $k \gg 2k_F$. This general behavior has already been discussed in detail for the case of $B = 0$ in Ref. 22. For $n \leqslant 2$, the scattering length never drops below the distance between BE and BC ($L_{EC} \simeq 840$ nm). This explains the overall weaker amplification (smaller $|I_{side}|$), which we observe at $B = 4.7$ T compared to the case of $B = 0$ [compare Figs. 2(c) and 3(a)]. It can be qualitatively understood since the width of the quasi-one-dimensional channel shrinks with increasing magnetic field and the phase space for electron-electron scattering is hence reduced. The $n = 3$ curve apparently converges to the zero field curve at large E_{kin} while at low E_{kin} large differences remain. This behavior expresses the fact that, at high energies, forward scattering dominates, which resembles scattering in a one-dimensional channel. Our calculations suggest that the differences in the electron-electron scattering dynamics between the one- and two-dimensional cases disappear at high E_{kin} and $n \geqslant 3$. In Fig. 4, at low energies, the scattering length at small filling fractions ($n = 1,2,3$) differs from its 2DES counterpart for $B = 0$ ($n \to \infty$). The origin of this discrepancy is the altered dispersion, yielding a different asymptotic behavior of the appropriate susceptibilities χ within the particle-hole continuum. Hence, this technical discrepancy at small energies should not be mistaken for a realistic prediction.

In summary, the calculated scattering length $l_{e\text{-}e}$ plotted in Fig. 4 explains several aspects of the measured magnetic-field dependence expressed in our data in Figs. 2(c) and 3(a). The increase of $l_{e\text{-}e}$ with increasing magnetic field causes the measured overall weaker amplification at finite B. The similarity of the calculated $l_{e\text{-}e}(E_{kin})$ curves for different values of B explains the overall similar behavior (except for phonon-induced effects) observed at different perpendicular magnetic fields. The calculations, in particular, predict that amplification should occur even at high perpendicular magnetic fields (up to $n = 1$), while the strongest amplification is expected for $B \to 0$ ($n > 3$) where we find a broad minimum of $l_{e\text{-}e} < L_{EC}$. The calculations suggest a transition toward one-dimensional scattering to happen for $n \leqslant 3$. The increase of $l_{e\text{-}e}$ with increasing magnetic field in this regime, especially at large energies, suggests that the region of amplification should be restricted to lower energies. This corresponds to the narrowing of the main minimum of I_{side} toward lower $|eV_E|$ in a finite perpendicular magnetic field. The ballistic regime visible in Figs. 2(c) and 3(a) as extended areas of $I_{side} \simeq 0$ in the limit of large $|eV_E|$ is expected for $l_{e\text{-}e} \gg L_{EC}$. It can therefore be qualitatively explained by the calculated monotonic increase of $l_{e\text{-}e}$ at large $E_{kin} - E_F$ (Fig. 4).

We have succeeded in qualitatively explaining some of the differences between the data at zero versus finite perpendicular magnetic field by the comparison with our calculations of $l_{e\text{-}e}$. However, other features can only be understood by taking the relaxation of hot electrons via emission of optical phonons into account. In our experiment, the emission of optical phonons can be clearly seen as periodic oscillations of the measured currents (see Fig. 3), which is the subject of the next section.

V. EMISSION OF OPTICAL PHONONS

A. Correlation between electron-electron scattering and emission of optical phonons

Electrons carrying enough excess energy $E_{kin} - E_F$ can lose part of their energy by emitting an optical phonon. The electronic momenta in our experiments cover only about 10% of the first Brillouin zone. In this range of small wave vectors, optical phonons have an almost constant dispersion relation, with an energy of $E_{ph}(q) \simeq 36$ meV in GaAs.[15,17,18,42,43] We therefore expect the hot electrons to emit phonons with a fixed energy $E_{ph} \simeq 36$ meV and a wide range of momenta. In fact, the momentum transfer is only limited by the quadratic dispersion relation of the electrons, and the scattering cross section for the emission of optical phonons is accordingly large. Since their dispersion relation is flat, the emitted optical phonons have almost zero velocity. Their main decay channels are reabsorption by electrons or, more efficient, the emission of two acoustic phonons. The momenta of the resulting acoustic phonons are not confined to the plane of the 2DES; consequently, they tend to disappear into the three-dimensional crystal and have a negligible chance to be reabsorbed by the 2DES.

The oscillations in I_{side} and I_C as a function of V_E in Fig. 3(b) are clearly caused by the emission of optical phonons, as their period [see vertical lines in Fig. 3(b)] is close to the energy of the longitudinal-optical (LO) phonons in GaAs $E_{ph} \simeq 36$ meV. The oscillations occur because the number of optical phonons that can be emitted per hot electron increases one by one at integer multiples of E_{ph} if $|eV_E|$ is increased. At large magnetic fields, we have observed up to 11 of these oscillations, which implies the sequential emission of 11 optical phonons by the individual hot electrons. By averaging over several periods of the oscillations, we have determined the *energy of the LO phonons in GaAs* at a cryogenic temperature $T \sim 260$ mK with a high precision to be $E_{ph}^{exp} = (36.0 \pm 0.1)$ meV. This result implies that, in our experiments, the interaction between electrons and phonons is dominated by the bulk LO phonons. If other decay channels, e.g., interface optical phonons that have different energies,[44,45] were also important, the observed oscillations of I_{side} would appear more irregular. The coupling between the two-dimensional electron system in a GaAs/AlGaAs heterostructure and interface phonon modes is expected to be reduced compared to bulk modes because of the small probability function of the electrons at the interface.

I_C has local maxima and I_{side} local minima at integer multiples of E_{ph} [vertical lines in Fig. 3(b)], which correspond to a rigid relative phase of π between the oscillations of the two currents. However, in Fig. 3(b), this behavior is caused by the way the data are depicted, namely, for a fixed I_E. In fact, $I_{side} + I_C = I_E =$ const. determines the phase between I_{side} and I_E. To overcome this limitation, we therefore replot the raw data [see inset of Fig. 3(a)] as a function of $V_{BE} - V_{BE,0}(V_E)$ in Fig. 5(a).

For comparison, Fig. 5(b) reproduces the plot for constant I_E already shown in Fig. 3(a). $V_{BE,0}(V_E)$ is defined as the

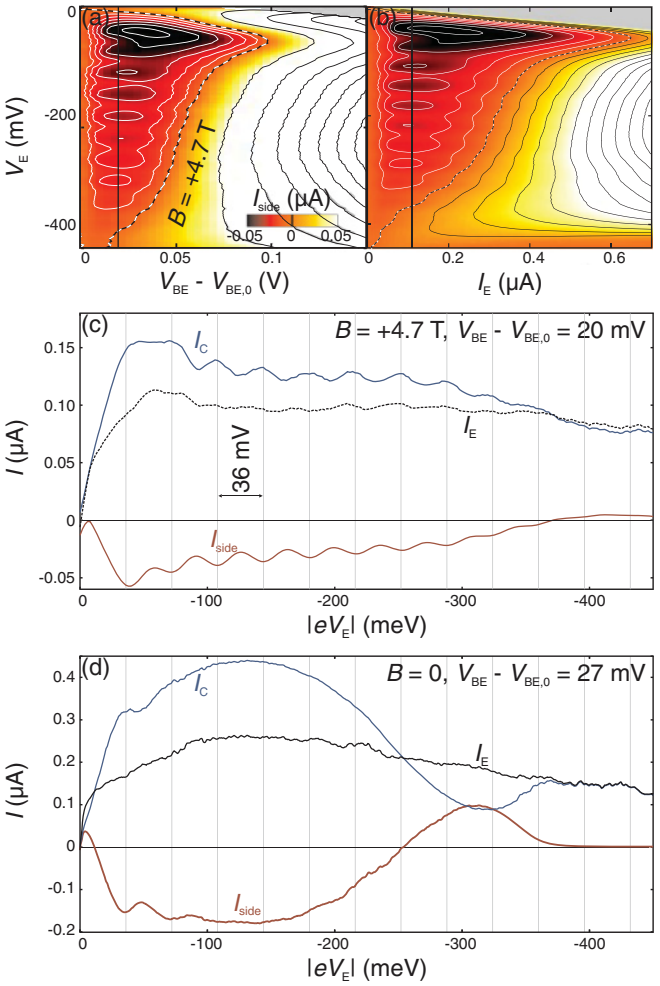

FIG. 5. (Color online) (a) Same data as in the inset of Fig. 3(a) but as a function of reduced gate voltage $V_{BE} - V_{BE,0}(V_E)$ instead of I_E (see main text for details). (b) Reproduction of Fig. 3(a) to allow a direct comparison. (c) Vertical traces of (a) at $V_{BE} - V_{BE,0} = 20$ mV as a function of $|eV_E|$ for all three currents. Integer multiples of $|eV_E| = 36$ meV are marked by vertical lines. (d) Traces analogous to (c), but for $B = 0$ (Fig. 2) and $V_{BE} - V_{BE,0} = 27$ mV.

gate voltage at which the emitter opens for a given V_E, and current starts to flow ($I_E > 0$). Compared to the choice of a constant I_E this processing technique does not require a rigid phase relation between I_{side} and I_C. The disadvantage is a small uncertainty regarding an offset of V_E which, however, does not effect the relation between I_{side} and I_C. Figure 5(c) shows a vertical trace of Fig. 5(a) at $V_{BE} - V_{BE,0} = 20$ mV and Fig. 5(d) an analogous graph for $B = 0$. Interestingly, the rigid phase difference of π between the phonon-induced oscillations in I_{side} and I_C remains (independent of B). This expresses a direct linkage between I_{side} and I_C caused by electron-electron scattering, which in itself is correlated to the emission of optical phonons.

Regardless of the value of B, the emitter current, which is no longer fixed, steeply grows at first as the emitter voltage V_E is increased. At $B = 0$, I_E then develops a broad maximum at $|eV_E| \sim 140$ meV [Fig. 5(d)]. The gradual decrease of I_E at $|eV_E| > 140$ meV is caused by an increase of the overall resistance. This is linked to an increase of the electron-phonon scattering rate with growing excess energy. At $B = 4.7$ T, I_E is further reduced and, interestingly, stays roughly constant in the regime of strong phonon-induced oscillations of I_C and I_{side}. A closer look reveals that I_E is slightly modulated and decreases stepwise at integer multiples of E_{ph} [vertical lines in Fig. 5(c)]. This weak modulation can be explained as an incremental increase of the overall device resistance whenever additional optical phonons contribute to electron scattering. It is a relative small effect since the device resistance is dominated by the almost pinched-off emitter.

The oscillations of I_C and I_{side} (at finite B) are much stronger and can not be explained in terms of the weak modulation of the overall resistance. Instead, they express the correlated dynamics of electron-phonon and electron-electron scattering. At relatively small excess energies $|eV_E| < 36$ meV, the collector current I_C steadily increases and exceeds the emitter current $I_C > I_E$ while the side current decreases accordingly, becoming negative. This avalanche amplification effect has been discussed in detail in Secs. III and IV. In short, the increase in amplification is caused by the decrease of $l_{e\text{-}e}$ as $|eV_E|$ is increased. At $B = 4.7$ T, the amplification is reduced compared to $B = 0$, while the emission of optical phonons has become an important scattering process [oscillations in Fig. 5(c)]. In the extreme case, the hot electrons will first emit as many optical phonons as possible and therefore end up with an energy less than E_{ph} before most of the electron-electron scattering occurs. As expected for such a scenario, the negative side current $I_{side}(|eV_E|)$ reaches its absolute minimum at $|eV_E| \simeq 36$ meV, just before the first optical phonon can be emitted. For higher energies $|eV_E|$ the side current then oscillates with local minima at integer multiples of E_{ph} where yet another optical phonon can be emitted.

Our calculations presented in the previous section suggest that $l_{e\text{-}e}$ increases with increasing perpendicular magnetic field as electron-electron scattering becomes weaker due to the transition from two-dimensional to quasi-one-dimensional scattering. We will see that the emission rate of optical phonons increases under the transition from two to one dimensions.[46,47] Our observation that the scattering with optical phonons takes over from electron-electron scattering as the perpendicular magnetic field is increased can therefore be interpreted as an indication for a transition from two- to one-dimensional scattering.

B. Magnetic-field dependence of the electron-phonon scattering time

In the following, we estimate the electron-phonon scattering time τ_{e-ph} by counting phonon-induced oscillations of I_{side} as a function of $|eV_E|$. Until now, we have assumed that if the electron-phonon scattering length is much smaller than the electron-electron scattering length ($l_{e-ph} \ll l_{e\text{-}e}$), the maximum possible number of optical phonons $n_{ph}^{max} = \text{int}(\frac{|eV_E|}{E_{ph}})$ will be emitted first. Afterward, hot electrons with the reduced excess energy $E_{kin} - E_F = |eV_E| - n_{ph}^{max} E_{ph} < E_{ph}$ will scatter with the 2DES. While this assumption seems reasonable for a rough picture, it disregards the influence of the sample's geometry on the correlation between the emission of LO phonons and electron-electron scattering, namely, that only scattering processes happening in the region between

emitter BE and collector barrier BC contribute to the observed amplification effect. The apparent decrease of the amplitude of the phonon-induced oscillations at large energies $|eV_E|$ [Fig. 5(c)] is related to this geometrical restriction.

Consider the length of the path $L(B) \geqslant L_{EC}$ that an electron subjected to a perpendicular magnetic field travels along the mesa edge from BE to BC. Assuming that backscattering of the hot electrons is strongly suppressed in a large perpendicular magnetic field (the extreme case is the Landauer-Büttiker edge channels, which only allow forward scattering), we can make an accurate statement. Phonon-induced oscillations with undiminished amplitude will be observed if (1) $l_{e\text{-}e} \gtrsim L$ (as is the case in our sample) and (2) $n_{ph}(L) \leqslant n_{ph}^{max}$. Here, $n_{ph}(L)$ is the number of phonons already emitted when the electron reaches BC.

In order to roughly estimate the electron-phonon scattering time τ_{e-ph} from our measurements in different magnetic fields, we now completely neglect all other energy relaxation processes including electron-electron scattering. We can then express the velocity of a hot electron with initial kinetic energy $E_{kin}^0 = |eV_E| + E_F$ after emission of k phonons as

$$v_k = \sqrt{\frac{2\left(E_{kin}^0 - kE_{ph}\right)}{m_{eff}}}. \tag{5}$$

The mean distance a hot electron travels until it has emitted n_{ph} optical phonons is

$$l(n_{ph}) = \sum_{k=0}^{n_{ph}-1} v_k \tau_{e-ph}(v_k) = \tau_{e-ph} \sum_{k=0}^{n_{ph}-1} v_k . \tag{6}$$

In the last step, we assumed for simplicity that $\tau_{e-ph}(v_k) \equiv \tau_{e-ph}$ is independent of the energy of the electron (as long as $E_{kin} - E_F > E_{ph}$), which is justified by previous calculations suggesting only a weak energy dependence.[47]

The expectation that, on average, n_{ph} phonons have already been emitted after the hot electron has traveled the distance L is expressed in the inequality $l(n_{ph}) \leqslant L < l(n_{ph}+1)$, which leads to the approximation

$$\begin{aligned} L &\simeq \frac{1}{2}[l(n_{ph}) + l(n_{ph}+1)] \\ &= \tau_{e-ph}\left(\sum_{k=0}^{n_{ph}-1} v_k + \frac{1}{2} v_{n_{ph}}\right). \end{aligned} \tag{7}$$

Inserting Eq. (5) and solving for τ_{e-ph} results in

$$\tau_{e-ph} = \frac{L\sqrt{m_{eff}/2}}{\sum_{k=0}^{n_{ph}-1}\sqrt{E_{kin}^0 - kE_{ph}} + \frac{1}{2}\sqrt{E_{kin}^0 - n_{ph}E_{ph}}}. \tag{8}$$

We estimate the distance the electrons travel to reach the collector barrier (by going along the edge) to be about $L(B) \simeq 1.5\ \mu$m [compare Fig. 1(a)] for the magnetic-field values considered here; for $B = 0$, no transport along the edge is expected and $L = L_{EC}$ is used instead.

Figure 6 shows the measured I_{side} as a function of V_E for several magnetic fields at an injected current $I_E = 100$ nA. Assuming that the emission of optical phonons is indeed by far the most efficient scattering process for hot electrons with $E_{kin} > E_F + E_{ph}$, we expect a constant oscillation amplitude

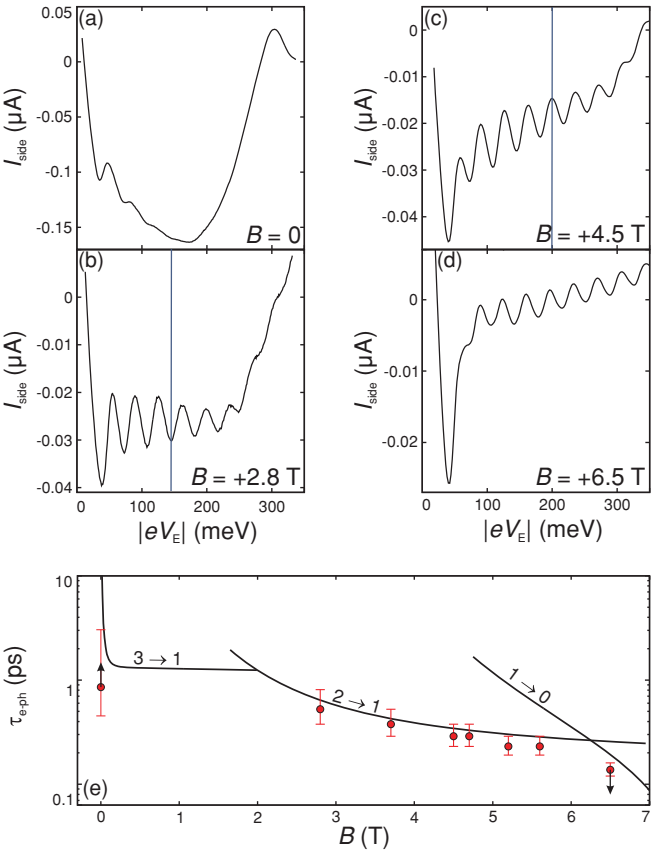

FIG. 6. (Color online) I_{side} as a function of $|eV_E|$ at constant $I_E = 100$ nA as in Figs. 3(b) and 3(c) for various perpendicular magnetic fields. The vertical lines in (b) and (c) mark the value of $|eV_E|$ above which the amplitude of the phonon-induced oscillations starts to decrease considerably. For (a) and (c), these values of $|eV_E|$ are outside of the plots. (e) Scattering times displayed in Table I as a function of magnetic field [determined from (a)–(d) and additional measurements]. The leftmost (rightmost) data point represents a lower (upper) limit as indicated by arrows (see Table I). The solid lines show theory curves obtained by heuristic application of Bockelmann's theory (numerical calculations, no fit parameters involved). The three branches belong to transitions between electronic subbands ($3 \to 1$, $2 \to 1$, $1 \to 0$) in the x direction via the emission of an optical phonon.

of I_{side} as long as $n_{ph}^{max} < n_{ph}(L)$. This means that all optical phonons that are energetically allowed are emitted before the electron reaches the collector barrier. Accordingly, we can interpret an onset of a decrease of the oscillation amplitude of I_{side} as a function of $|eV_E|$ as the electron energy at which $n_{ph}(L) \simeq n_{ph}^{max}$. This energy is marked in Figs. 6(b) and 6(c) by vertical lines and corresponds to $E_{kin}^0 = E_F + n_{ph}^{max}E_{ph} = E_F + n_{ph}(L)\,E_{ph}$. Inserting this relation into Eq. (8) then yields

$$\tau_{e-ph} = \frac{L\sqrt{m_{eff}/2}}{\sum_{k=1}^{n_{ph}}\sqrt{E_F + kE_{ph}} + \frac{1}{2}\sqrt{E_F}}, \tag{9}$$

which can be used to calculate τ_{e-ph} from the data for different magnetic fields.

For $B = 0$ [Fig. 6(a)], the phonon-induced oscillations quickly weaken as the excess energy $|eV_E|$ is increased. We interpret the absence of a constant oscillation amplitude

TABLE I. Estimated number of optical phonons $n_{ph}(L)$ emitted within the distance L that hot electrons travel between emitter and collector [for the algorithm of determining $n_{ph}(L)$, see Fig. 6]. The electron-phonon scattering times τ_{e-ph} are then calculated with Eq. (9).

B (T)	0	2.8	3.7	4.5	4.7	5.2	5.6	6.5
n_{ph}	$\lesssim 1$	3	4	5	5	6	6	$\gtrsim 9$
τ_{e-ph} (ps)	$\gtrsim 0.85$	0.52	0.38	0.29	0.29	0.23	0.23	$\lesssim 0.14$

as a scattering time that exceeds the calculated value for $n_{ph}(L) = 1$. In addition, for $B = 0$, our assumption of forward scattering only does not hold, which tends to increase the effective L. Hence, our model tends to underestimate τ_{e-ph} for $B = 0$. For $B = 6.5$ T [Fig. 6(d)], the oscillation amplitude is constant over the whole energy range measured, showing nine oscillations, so we conclude $n_{ph}(L) \geqslant 9$. The values for $n_{ph}(L)$ and τ_{e-ph} obtained from the data for different magnetic fields shown in Figs. 6(a)–6(d) and similar measurements are summarized in Table I.

In Fig. 6(e), τ_{e-ph} (logarithmic scale) is plotted as a function of the magnetic field. The error bars express the uncertainty in determining $n_{ph}(L)$ taken to be $\Delta n_{ph} = 1$. For the two extremal values, $B = 0$ and 6.5 T, the plotted values of τ_{e-ph} represent a lower ($B = 0$) and upper ($B = 6.5$ T) limit, respectively.

In summary, we observe a dramatic decrease of τ_{e-ph} by more than an order of magnitude as the perpendicular magnetic field is increased from zero to a filling fraction beyond $n = 1$.

C. Theoretical analysis of electron-phonon scattering

The interaction between hot electrons and optical phonons in nanostructures has been investigated theoretically in detail with and without applied perpendicular magnetic field.[36,46–49]

Extending the calculations of Bockelmann *et al.*,[46] Telang *et al.*[47] investigated the effect of a magnetic field on the electron-phonon scattering rate in quasi-one-dimensional systems rigorously by solving the Schrödinger equation with boundaries. They found that the scattering rate only weakly depends on the electron energy in a quasi-one-dimensional channel. Relying on this weak energy dependence, for convenience, here we numerically integrate Bockelmann's formula for a fixed initial energy of $E_{kin} = 82$ meV of the injected electron. This energy value has been chosen to be similar to the one used in Ref. 17 where the electron-phonon scattering time in a vertical tunneling structure is calculated for zero magnetic field (their result of $l_{e-ph} = 0.24$ ps is not applicable to our case, though, since we have a lateral nanostructure in a 2DES).

We use the edge-channel diameter $R_c = \sqrt{2(n+0.5)}\, l_c$ as the lateral confinement width. The x component of the phonon momenta (along the direction of electron confinement) can be treated as a continuum since $L_x \gg R_c$. We assume the electrons to occupy the lowest perpendicular subband $k_z \to 0$ (compare last paragraph of Sec. III), hence, phonon emission mainly occurs within the plane of the 2DES. The solid lines in Fig. 6(e) express our numerical results for $\tau_{e-ph}(B)$. They are in excellent agreement with experimental data even though they contain no free parameters. These theory curves correspond to three branches of intersubband scattering (subbands in the x direction) under emission of an optical phonon. Most experimental data points lie just below the lowest branch, which is expected if the overall scattering rate is dominated by the fastest process [lowest branch Fig. 6(e)] with a slight contribution of slower processes (higher branches). The transitions between the three branches result from the according discontinuities in the electronic one-dimensional density of states (see Bockelmann's results[46]). These jumps have been observed and discussed in detail in numerical calculations by Telang *et al.*[47]

VI. INFLUENCE OF THE MAGNETIC-FIELD DIRECTION

Until now, only perpendicular magnetic fields that guide the injected electrons away from the side contact have been discussed ($B > 0$). In this section, the discussion is extended to the opposite field direction ($B < 0$) that tends to direct the injected electrons into the side contact [compare Figs. 7(d) and 7(e)]. In a naïve model, one would expect $I_{side} \equiv I_E$ (and $I_C = 0$) for $B < 0$ as long as $|B|$ is large enough to confine the current to edge channels, and for a perfect side contact without reflection.

Figures 7(a) and 7(b) show measurements of I_{side} as a function of V_E and (relatively small) I_E for opposite field directions $B = \pm 2.8$ T. All other parameters are kept equal (the color scale has been adapted, though). As in the previous figures, white contour lines denote $I_{side} < 0$, while for black lines, $I_{side} > 0$. Vertical traces (for constant I_E) including the respective absolute minimum of I_{side} are plotted in Fig. 7(c) for both magnetic-field directions $B = \pm 2.8$ T as well as for $B = 0$.

The naïve expectation $I_{side} = I_E$ for $B < 0$ based on edge-channel transport is clearly not fulfilled. Instead, we observe both oscillations of I_{side} induced by the emission of optical phonons and amplification ($I_{side} < 0$). Nevertheless, the differences for opposite magnetic-field directions are striking. For $B < 0$, the phonon-induced oscillations decrease much quicker as $|eV_E|$ is increased and the region of amplification ($I_{side} < 0$) is much smaller. In addition, the maximum amplification effect [absolute mimimum of I_{side} marked by V_E^{min} in Fig. 7(c)] occurs at a much larger energy $|eV_E^{min}| \simeq 250$ meV for $B < 0$ compared to $|eV_E^{min}| \simeq 35$ meV for $B > 0$. The absolute minimum for $B = 0$ occurs between these two values at $|eV_E^{min}| \simeq 180$ meV. For even more negative magnetic fields, I_{side} stays positive for all $|eV_E|$, thus, no amplification effect can be observed at all. This can be seen in Fig. 8, which shows the $B = -2.8$ T trace from Fig. 7(c) as well as measurements for $B = -3.5$ and -5.2 T. The latter field is large enough to prevent amplification ($I_{side} > 0$).

The Landauer-Büttiker edge-channel picture is limited to linear-response transport for $|E_{kin} - E_F| \ll E_F$, and is therefore not appropriate to describe our data at $|eV_E| \gg E_F$. In this nonlinear regime, scattering of the hot electrons, incomplete screening of the Lorentz force acting on hot electrons in the bulk of the 2DES, and the energy-dependent cyclotron radius have to be accounted for. In the following, we develop a semiclassical approach to model the magnetic-field dependence far from equilibrium. As before, we assume that the cyclotron radius $R_c = \frac{\sqrt{2m_{eff}E_{kin}}}{|eB|}$ roughly defines the width

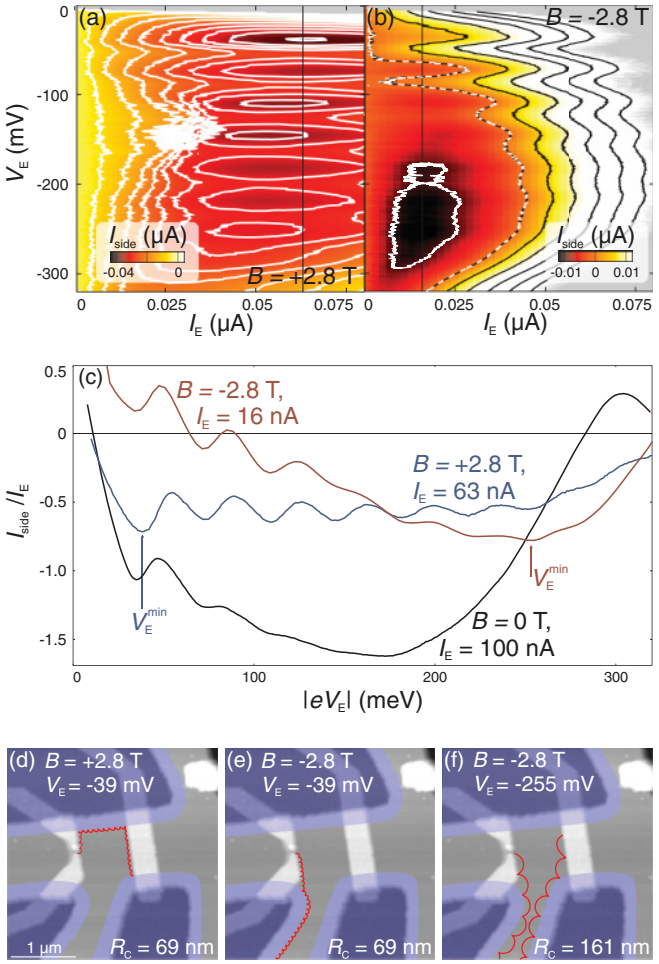

FIG. 7. (Color online) (a), (b) I_{side} as a function of I_E and V_E as in Fig. 3, for $V_{BC} = -280$ mV($E_{BC} = E_F - 1.4$ meV) at perpendicular magnetic fields of $B = 2.8$ and -2.8 T. Contour lines are spaced by 5 nA. (c) Vertical traces (I_{side}/I_E is plotted as a function of $|eV_E|$) through the absolute minimum of I_{side} for three different magnetic fields: $B = 2.8$ T at $I_E = 16$ nA [from (a)], $B = -2.8$ T at $I_E = 63$ nA [from (b)], and $B = 0$ at $I_E = 100$ nA [from data similar to Fig. 3(a), but for $V_{BC} = -280$ mV as in (a) and (b)]. (d)–(f) Sketches of the classically expected skipping orbit motion of hot electrons with energies of (d), (e) $|eV_E| = 39$ meV and (f) $|eV_E| = 255$ meV corresponding to the absolute minima of I_{side} at $B = \pm 2.8$ T. A zone of depletion extending an estimated 200 nm from the etched edges into the Hall bar is marked in blue.

of the channel in which most of the hot electrons move along the edge of the 2DES. This is assured by the large Lorentz force acting on the hot electrons, which forces them back to the edge even after scattering.

The cyclotron radius at the energy $|eV_E^{min}| \simeq 35$ meV of the absolute minimum of I_{side} for $B = +2.8$ T is $R_c \simeq 69$ nm, still relatively small. Hence, the electrons move along the edge in a narrow channel as sketched in Fig. 7(d). For the reversed magnetic field $B = -2.8$ T, electrons are guided toward the side contact as shown in Fig. 7(e). This should lead to $I_{side} = I_E$, and indeed I_{side} becomes positive for relatively small $|eV_E| \lesssim 100$ meV, where we observe the maximum amplification for $B > 0$ [Fig. 7(c)]. Figure 7(f) sketches the situation at an energy of $|eV_E^{min}| \simeq 250$ meV, corresponding

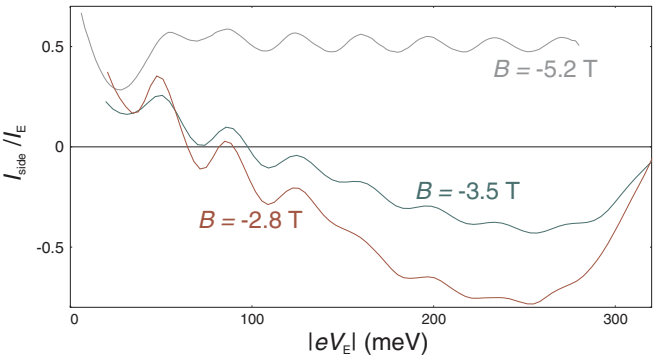

FIG. 8. (Color online) I_{side}/I_E versus $|eV_E|$ for constant $I_E = 15$ nA. Included is a measurement for $B = -2.8$ T as already shown in Fig. 7(c) and two additional curves for $B = -3.5$ and -5.2 T measured at $V_{BC} = -265$ mV ($E_{BC} = E_F - 1.8$ meV). The slightly different collector barrier height for $B = -2.8$ T of $E_{BC} = E_F - 1.4$ meV is not important for the qualitative behavior of interest here.

to $R_c = 161$ nm at $B = -2.8$ T. At this energy, $2R_c$ is already comparable to the width of the side contact and energy exchange between the two edge channels with opposite current direction can occur. As a result, excited electrons can reach the collector barrier and amplification can occur similarly to $B > 0$. Furthermore, within the region of backscattering (at the "mouth" of the side contact), electron-electron scattering is enhanced as the two "edge channels" of opposite direction tend to merge into a region without a preferred direction. For large energies $|eV_E|$ the side current therefore becomes more negative for $B < 0$ compared to $B > 0$.

Our semiclassical model based on edge transport of hot electrons in a strong perpendicular magnetic field fails to explain one crucial observation, though. In the region of relatively small energies $|eV_E| \lesssim 100$ meV, where $I_{side} > 0$ for $B < 0$, we observe phonon-induced oscillations, while our model does *not* propose such an effect since it assumes that all current-carrying electrons are guided toward the side contact. In this case, the emission of optical phonons should not influence the number of hot electrons reaching this contact. Even backscattering at a nonperfect ohmic contact, which is in our case one millimeter away, would not allow such a behavior since, after having traveled such a distance, all electron-hole pairs would have recombined within the edge channel, and no effects caused by phonon emission should be visible. In addition, we would expect to see $I_{side} = I_E$, but Fig. 7(c) shows that this is not the case. The observation of phonon-induced oscillations in this regime points toward leakage of energy into bulk states related to the emission of optical phonons by hot electrons moving along the edge. However, free hot electrons scattered into the bulk of the 2DES tend to be directed back to the edge of the 2DES by the Lorentz force acting on them. This contradiction can be resolved by taking localized bulk states into account, which are a result of disorder combined with reduced screening in a magnetic field. A hot electron can travel from BE to BC by a combination of energy relaxation and hopping between these localized states. Our experimental observations are consistent with the assumption that, in a large magnetic field, a small part of the overall current is carried by

such a hopping transport mechanism. Finally, we observe that the amplitude of the phonon-induced oscillations decays faster as the energy $|eV_E|$ is increased for $B < 0$ compared to $B > 0$. This behavior might be related to the transport via localized states, but will not be discussed in detail here.

VII. CONCLUSIONS

In conclusion, we have studied the energy relaxation of hot electrons injected at an energy $E_{kin} \gg E_F$ into an otherwise degenerate 2DES. The transport measurements have been performed in a mesoscopic three-terminal device in which two of the contacts (emitter and collector) are separated by tunable electrostatic barriers. The emitter current and the energy of the injected electrons are fully controlled while the currents into the other two contacts are measured. Our main observation is that, as a function of a perpendicular magnetic field, the electron-electron scattering rate decreases, while the emission of optical phonons increases drastically. Quantitatively, the corresponding electron-phonon relaxation time declines from over 0.85 ps at zero magnetic field to below 0.14 ps at strong perpendicular magnetic fields. Numerical calculations within the theoretical standard approaches quantitatively confirm our data and support the following interpretation of our experiments. We have observed the transition from two-dimensional scattering of hot electrons at zero magnetic field toward one-dimensional dynamics at large perpendicular magnetic fields. In the quasi-one-dimensional limit, the interaction of hot electrons with optical phonons becomes so strong that we clearly observe the emission of more than 10 optical phonons by individual hot electrons in the current signals. This allows us to determine the onset energy of LO phonons in GaAs at $T \simeq 260$ mK with high precision to $E_{ph} = 36.0 \pm 0.1$ meV. Finally, measurements as a function of the direction of a strong perpendicular magnetic field suggest that the expected flow of the hot electrons along the mesa edges is accompanied by a second transport contribution, which we interpret as hot electrons hopping between localized bulk states of the 2DES.

ACKNOWLEDGMENTS

We thank J. P. Kotthaus and A. Govorov for helpful discussions. Financial support by the German Science Foundation via SFB 631, LU 819/4-1, and the German Israel program DIP, the German Excellence Initiative via the "Nanosystems Initiative Munich (NIM)", and LMUinnovativ (FuNS) is gratefully acknowledged.

APPENDIX: CURRENT DEPENDENCE

The main focus of this article is to study I_{side} as a function of the kinetic excess energy $|eV_E|$ of the injected electrons. Figure 9 shows the side current I_{side} as a function of I_E for $B = 0$ (left panel) as well as for $B = 5.2$ T (right panel). The $B = 0$ data have already been discussed in Ref. 22. Data for $|eV_E| \leqslant 100$ meV are plotted in Fig. 9(a). In this low-energy regime, I_{side} first rapidly decreases as a function of I_E before it grows again for larger currents. Strikingly, for $I_{side} > 200$ nA, all curves measured at energies below $|eV_E| = 100$ meV follow the same straight line, which is actually parallel to the line

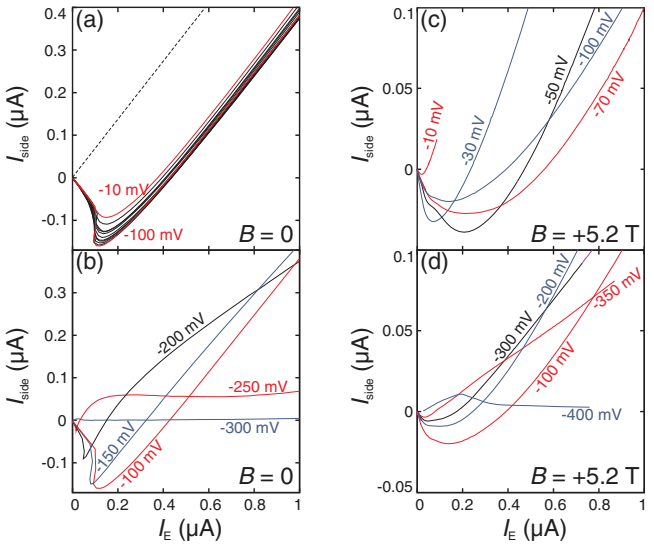

FIG. 9. (Color online) I_{side} as a function of I_E for several values of V_E (given in the plot); $V_{BC} = -265$ mV($E_{BC} = E_F - 1.8$ meV). $B = 0$ in (a) and (b) and $B = 5.2$ T in (c) and (d). Curves for relatively low excess energies 10 meV $\leqslant |eV_E| \leqslant$ 100 meV [equal spacings of 10 meV in (a) and energies as marked in (c)] are plotted in (a), (c), while the plots in (b), (d) concentrate on $|eV_E| \geqslant 100$ meV (energies marked).

expected for ohmic behavior [dashed line in Fig. 9(a)].[22] This curve shape can be interpreted as an ohmic contribution to I_{side} (which is proportional to I_E and is determined by the ohmic resistances of the three-terminal device) plus a negative contribution that saturates at $I_{side} \simeq -0.2$ μA. The saturation of the negative contribution to I_{side} is explained by taking into account the neutralization of electron-hole pairs created by electron-electron scattering. The generation rate of the electron-hole pairs should be roughly proportional to the number of injected electrons, so neutralization becomes more efficient at larger I_E. This is related to the positive charge building up between BE and BC due to the amplification effect, which hinders the escape of hot electrons via BC. Since electrons that can not escape add to the neutralization of holes, a steady state is reached in which the negative contibution to I_{side} saturates.[22]

The ohmic contribution of I_{side} proportional to I_E is straightforward to explain. At energies at which the electron-electron scattering length $l_{e\text{-}e}$ is small, multiple scattering processes result in many electrons with small kinetic energies and almost arbitrary direction of their momentum. These electrons mimic a diffusive motion, the prerequisite for an ohmic behavior.[22]

The regime of high energies $|eV_E| \geqslant 100$ meV is depicted in Fig. 9(b). Here, we observe the transition to $l_{e\text{-}e}$ being longer than the device dimensions, which, in its extremes, results in $I_{side} = 0$ (observed at $|eV_E| = 300$ meV) because the hot electrons move ballistically through the sample.[22]

In a strong perpendicular magnetic field, the amplification effect is reduced, hence, Fig. 9(c) has a differently scaled y axis. The preferred directional motion along the edges of the Hall bar at $B = 5.2$ T prevents ohmic contributions even at large currents. This explains part of the more complex behavior seen for low energies $|eV_E| \leqslant 100$ meV in Fig. 9(c)

at $B = 5.2$ T, namely, that the bunching of curves $I_{\text{side}}(I_{\text{E}})$ for several energies at high I_{E} is missing. In addition, in a large positive magnetic field, the minimum of I_{side} strongly shifts as a function of energy and $I_{\text{side}} < 0$ persists to larger I_{E} and larger energies $|eV_{\text{E}}|$ compared to $B = 0$ [compare Figs. 9(c) and 9(d)]. A detailed discussion of these effects, which reflect the more complex situation in a strong perpendicular magnetic field including the enhanced emission of optical phonons, would be very difficult. In a positive magnetic field, the high-energy limit $I_{\text{side}} = 0$ is reached at a larger $|eV_{\text{E}}|$ as for $B = 0$ [see also Figs. 2(c) and 3(a)]. This tendency might be understood in terms of the stronger interaction with optical phonons, which shifts the regime of ballistic motion throughout the Hall bar toward higher velocities of the injected electrons.

[1] G. J. Schinner, H. P. Tranitz, W. Wegscheider, J. P. Kotthaus, and S. Ludwig, Phys. Rev. Lett. **102**, 186801 (2009).
[2] V. S. Khrapai, S. Ludwig, J. P. Kotthaus, H. P. Tranitz, and W. Wegscheider, Phys. Rev. Lett. **97**, 176803 (2006).
[3] V. S. Khrapai, S. Ludwig, J. P. Kotthaus, H. P. Tranitz, and W. Wegscheider, Phys. Rev. Lett. **99**, 096803 (2007).
[4] V. S. Khrapai, S. Ludwig, J. P. Kotthaus, H. P. Tranitz, and W. Wegscheider, J. Phys. Condens. Matter **20**, 454205 (2008).
[5] U. Gasser, S. Gustavsson, B. Kung, K. Ensslin, T. Ihn, D. C. Driscoll, and A. C. Gossard, Phys. Rev. B **79**, 035303 (2009).
[6] D. Harbusch, D. Taubert, H. P. Tranitz, W. Wegscheider, and S. Ludwig, Phys. Rev. Lett. **104**, 196801 (2010).
[7] M. G. Prokudina, V. S. Khrapai, S. Ludwig, J. P. Kotthaus, H. P. Tranitz, and W. Wegscheider, Phys. Rev. B **82**, 201310(R) (2010).
[8] H. J. Stocker, H. Levinstein, and C. R. Stannard, Phys. Rev. **150**, 613 (1966).
[9] H. J. Stocker and H. Kaplan, Phys. Rev. **150**, 619 (1966).
[10] J. Barker and C. Hearn, Phys. Lett. A **29**, 215 (1969).
[11] R. E. Nahory, Phys. Rev. **178**, 1293 (1969).
[12] J. Kuhl and W. E. Bron, Solid State Commun. **49**, 935 (1984).
[13] Y. Katayama and K. F. Komatsubara, Phys. Rev. Lett. **19**, 1421 (1967).
[14] B. C. Cavenett, Phys. Rev. B **5**, 3049 (1972).
[15] T. W. Hickmott, P. M. Solomon, F. F. Fang, F. Stern, R. Fischer, and H. Morkoc, Phys. Rev. Lett. **52**, 2053 (1984).
[16] P.-F. Lu, D. C. Tsui, and H. M. Cox, Phys. Rev. Lett. **54**, 1563 (1985).
[17] M. Heiblum, D. Galbi, and M. Weckwerth, Phys. Rev. Lett. **62**, 1057 (1989).
[18] U. Sivan, M. Heiblum, and C. P. Umbach, Phys. Rev. Lett. **63**, 992 (1989).
[19] I. I. Kaya and K. Eberl, Phys. Rev. Lett. **98**, 186801 (2007).
[20] U. Sivan, M. Heiblum, and C. P. Umbach, Phys. Rev. Lett. **63**, 992 (1989).
[21] A. Palevski, M. Heiblum, C. P. Umbach, C. M. Knoedler, A. N. Broers, and R. H. Koch, Phys. Rev. Lett. **62**, 1776 (1989).
[22] D. Taubert, G. J. Schinner, H. P. Tranitz, W. Wegscheider, C. Tomaras, S. Kehrein, and S. Ludwig, Phys. Rev. B **82**, 161416(R) (2010).
[23] D. Taubert, G. J. Schinner, C. Tomaras, H. P. Tranitz, W. Wegscheider, and S. Ludwig, J. Appl. Phys. **109**, 102412 (2011).
[24] J. G. Williamson, H. van Houten, C. W. J. Beenakker, M. E. I. Broekaart, L. I. A. Spendeler, B. J. van Wees, and C. T. Foxon, Surf. Sci. **229**, 303 (1990).
[25] M. Büttiker, Phys. Rev. Lett. **57**, 1761 (1986).
[26] D. Pines and P. Nozières, *The Theory of Quantum Liquids* (Benjamin, New York, 1966), Vol. 1.
[27] G. Baym and C. Pethick, *Landau Fermi-Liquid Theory: Concepts and Applications* (Wiley, New York, 1999).
[28] G. Giuliani and G. Vignale, *Quantum Theory of the Electron Liquid* (Cambridge University, Cambridge, UK, 2005).
[29] G. F. Giuliani and J. J. Quinn, Phys. Rev. B **26**, 4421 (1982).
[30] A. L. Fetter, Ann. Phys. (NY) **88**, 1 (1974).
[31] C. S. Ting, S. C. Ying, and J. J. Quinn, Phys. Rev. Lett. **37**, 215 (1976).
[32] C. S. Ting, S. C. Ying, and J. J. Quinn, Phys. Rev. B **16**, 5394 (1977).
[33] S. Das Sarma and J. J. Quinn, Phys. Rev. B **25**, 7603 (1982).
[34] K. W. Chiu and J. J. Quinn, Phys. Rev. B **9**, 4724 (1974).
[35] M. P. Greene, H. J. Lee, J. J. Quinn, and S. Rodriguez, Phys. Rev. **177**, 1019 (1969).
[36] W. Gasser and U. C. Täuber, Z. Phys. B: Condens. Matter **69**, 87 (1987).
[37] K. Le Hur, Phys. Rev. B **74**, 165104 (2006).
[38] T. Giarmarchi, *Quantum Physics in One Dimension* (Clarendon, Oxford, 2006).
[39] M. P. A. Fisher and L. I. Glazman, in *Mesoscopic Electron Transport*, edited by L. Sohn, L. Kouwenhoven, and G. Schoen (Kluwer Academic, Dordrecht, 1996), p. 331.
[40] A. Imambekov and L. I. Glazman, Science **323**, 228 (2009).
[41] B. Kramer, in *Quantum Transport and Dissipation*, edited by T. Dittrich, G. Ingold, P. Hänggi, B. Kramer, G. Schoen, and W. Zwerger (Wiley, New York, 1998), p. 80.
[42] J. L. T. Waugh and G. Dolling, Phys. Rev. **132**, 2410 (1963).
[43] J. S. Blakemore, J. Appl. Phys. **53**, R123 (1982).
[44] P. A. Thiry, M. Liehr, J. J. Pireaux, R. Caudano, P. Lambin, J. P. Vigneron, A. A. Lucas, and T. Kuech, J. Vac. Sci. Technol. B **4**, 1028 (1986).
[45] Y.-M. Chang and N.-A. Chang, J. Appl. Phys. **93**, 2015 (2003).
[46] U. Bockelmann and G. Bastard, Phys. Rev. B **42**, 8947 (1990).
[47] N. Telang and S. Bandyopadhyay, Phys. Rev. B **48**, 18002 (1993).
[48] S. Das Sarma and A. Madhukar, Phys. Rev. B **22**, 2823 (1980).
[49] H. Bruus, K. Flensberg, and H. Smith, Phys. Rev. B **48**, 11144 (1993).